Discrete gap breathers in a diatomic Klein-Gordon chain: Stability and mobility

Andrey V. Gorbach* and Magnus Johansson[†]

Department of Physics and Measurement Technology (IFM), Linköping University, S-581 83 Linköping, Sweden
(Received 3 January 2003; published 26 June 2003)

A one-dimensional diatomic chain with harmonic intersite potential and nonlinear external potential is considered (the Klein-Gordon model). Localized solutions of the corresponding nonlinear differential equations with frequencies inside the gap of the linear wave spectrum—"gap breathers"—are studied numerically. The linear stability analysis for these solutions is performed while changing the system parameters from the anticontinuous to the continuous limit. Two different types of solutions are considered: symmetric centered at a heavy atom and antisymmetric centered at a light atom, respectively. Different mechanisms of instability, oscillatory as well as nonoscillatory, of the gap breathers are studied, and the influence of the instabilities on the breather solutions is investigated in the dynamics simulations. In particular, the presence of an "inversion of stability" regime, with simultaneous nonoscillatory instabilities of symmetric and antisymmetric solutions with respect to antisymmetric perturbations, is found, yielding practically radiationless mobility.

I. INTRODUCTION

During recent decades it has been realized that the intrinsic structure of a medium can significantly influence the properties of nonlinear excitations. In particular, new types of solitonlike localized nonlinear excitations were discovered in optical medium with spatially modulated refractive index—the so-called "gap" and "out-gap" solitons [1,2]. The frequency and wave number of a carrier wave in such excitations lie in the vicinity of the gap of the linear wave spectrum, which appears as a consequence of the space modulation of the system parameters. The unique structure and properties of gap and out-gap solitons are conditioned by the existence of two branches of the linear wave dispersion curve with opposite signs of dispersion. (For a review on optical gap and out-gap solitons, see Refs. [3,4]). Similar localized excitations can also exist in other systems with intrinsic structure, since the appearance of gaps in linear waves spectrum is a general effect in such media. By analogy with modulated optical systems, gap and out-gap solitons were discovered later in different modulated elastic and magnetic media (e.g., Refs. [5–9]). However, unlike the optical model, all these elastic and magnetic systems are discrete, and the continuous approximation (based on the assumption that the localization length of the excitation is much larger than the lattice spacing) together with a rotating wave approximation (RWA), neglecting the effect of generation of higher harmonics, were involved to obtain gap and out-gap soliton solutions.

On the other hand, localized nonlinear time-periodic solutions can exist in pure discrete systems, despite the fact that the corresponding mathematical models are nonintegrable [10]. These localized excitations—discrete breathers (or intrinsically localized modes)—were studied in different discrete systems, and several numerical methods were developed to obtain breather solutions (see for a review Refs.

[11,12]). The existence of discrete breathers in diatomic chains with nonlinear interatomic potentials [Fermi-Pasta-Ulam (FPU) models] was proved in Ref. [13]. Later, discrete breathers with frequencies inside the gap—*discrete gap breathers* (DGB)—were investigated numerically in diatomic FPU chains for some particular values of system parameters, and the linear stability analysis was performed for these breather solutions [14–16]. Recently, also the existence of discrete gap solitons in an array of weakly coupled optical waveguides with alternating widths was predicted and the conditions of their generation were studied numerically [17].

Discrete breathers can also be studied analytically near the so-called "anticontinuous" limit, when the localization length of the excitation becomes comparable to the lattice spacing. Several papers were devoted to analytical investigation of DGB in diatomic FPU chains within the RWA [16,18–21]. In Ref. [22], the same model was treated numerically within the RWA. The effect of the second harmonics on the DGB solutions was also studied in Ref. [23]. It was found that there can exist two types of gap breathers with symmetric and antisymmetric structures [18,19,21]. Numerical simulations performed in Refs. [19,21] have shown that symmetric gap breathers are stable at small values of the coupling constant, while antisymmetric gap breathers are unstable.

The stability of gap localized modes was also studied in the continuous massive Thirring model (which is similar to the optical model with spatially modulated refractive index) [24–26]. It was shown that in the continuous limit, gap solitons can possess oscillatory instabilities.

The purpose of the present paper is to connect the results of studies of DGB properties with those of gap solitons obtained within continuous models. In particular, it is of interest to investigate the stability of gap breathers in the complete regime of continuation from the anticontinuous to the continuous limit, and to compare the results with those obtained in pure discrete systems (for DGB) [14–16,19,21] and in continuous models (for gap solitons) [24–26]. It is also of interest to look for possible bifurcations of DGB solutions when varying the system parameters from the anti-

continuous to the continuous limit. Another important question concerns the mobility of gap breathers. Generally, the discreteness breaks the translational symmetry and significantly affects the mobility of excitations. This effect is usually interpreted through an additional Peierls-Nabarro barrier. This lead to the dissipation of energy of a moving excitation, which finally becomes trapped. However, in some cases, the Peierls-Nabarro barrier might become very small or even vanish, so that considerably increased mobility of breathers is expected [27]. The detailed study of the mobility properties of DGB's is of great importance to understand the possible role of such excitations in energy transfer processes.

The outline of this paper is as follows. In Sec. II, we introduce the model of a one-dimensional Klein-Gordon diatomic chain and briefly describe the properties of linear waves dispersion relation in this model. In Sec. III, the main ideas of the procedure of construction of breathers starting from the anticontinuous limit, originally developed in Refs. [12,28], are reviewed, and some particular features of this procedure when dealing with gap breathers are discussed. In Sec. IV, the numerical results on continuation, stability, and mobility of gap breathers are presented. The conclusions are made in Sec. V.

II. THE MODEL

We consider one of the simplest examples of a system with two bands in the linear waves spectrum: a one-dimensional diatomic chain with periodically distributed atoms of alternating masses m and M ($M > m$). The potential of interaction between atoms is taken to be harmonic,

$$U(\xi_n - \xi_{n-1}) = \frac{C}{2}(\xi_n - \xi_{n-1})^2, \qquad (1)$$

and a nonlinear external potential is added (the so-called Klein-Gordon model),

$$V(\xi_n) = \frac{\gamma_2}{2}\xi_n^2 + \frac{\gamma_4}{4}\xi_n^4, \qquad (2)$$

where ξ_n is the displacement of the nth atom from equilibrium and the constants C, γ_2, γ_4 are positive ($\gamma_4 > 0$ corresponds to the case of so-called "hard nonlinearity"). Thus, the equation of motion for the nth atom reads

$$\mu[1 + (-1)^n \delta^2]\ddot{\xi}_n + C(2\xi_n - \xi_{n+1} - \xi_{n-1})$$
$$+ \gamma_2\xi_n + \gamma_4\xi_n^3 = 0, \qquad (3)$$

where $\mu = (M + m)/2$ and $\delta^2 = (M - m)/(M + m)$.

The energy E of a nonlinear excitation can be written as the sum of the energy densities e_n of all the particles in the chain:
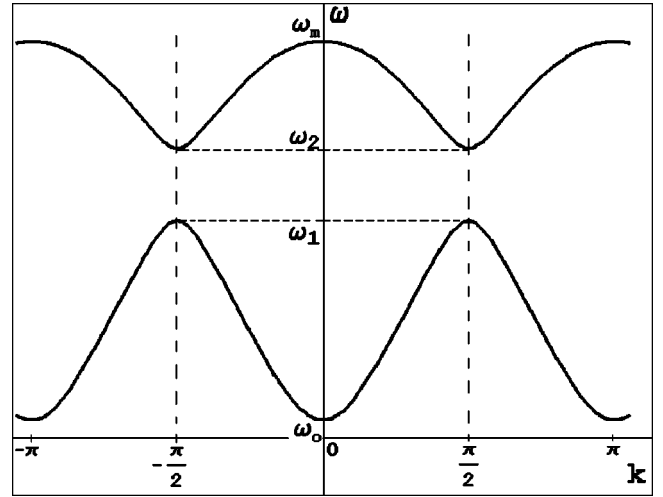
$$E = \sum_n e_n, \qquad (4)$$

FIG. 1. Dispersion law of linear waves (6) in a diatomic chain. Lattice spacing a is equal to unity.

$$e_n = \frac{\mu}{2}[1 + (-1)^n \delta^2]\dot{\xi}_n^2 + \frac{C}{4}[(\xi_n - \xi_{n-1})^2$$
$$+ (\xi_n - \xi_{n+1})^2] + \frac{\gamma_2}{2}\xi_n^2 + \frac{\gamma_4}{4}\xi_n^4. \qquad (5)$$

The dispersion law of linear waves in such a model is shown in Fig. 1 and can be described by the following characteristic equation:

$$\omega^4 - (\omega_1^2 + \omega_2^2)\omega^2 + \omega_1^2\omega_2^2 - \tilde{\omega}_1^2\tilde{\omega}_2^2\cos^2(ka) = 0, \qquad (6)$$

where

$$\omega_1 = \sqrt{(2C + \gamma_2)/M}, \qquad (7)$$

$$\omega_2 = \sqrt{(2C + \gamma_2)/m}$$

are the boundaries of the spectrum gap, $\tilde{\omega}_1^2 = 2C/M$, $\tilde{\omega}_2^2 = 2C/m$, k is the wave number, and a is lattice spacing, which we will put equal to unity in what follows. (Note that the gap width $\omega_2 - \omega_1$ increases with increasing coupling C.) We are interested in discrete breather solutions of the set of equations (3) with frequencies ω inside the gap of linear waves spectrum $\omega_1 < \omega < \omega_2$—gap breathers. In the following sections the numerical procedure of finding such solutions and the results of the linear stability analysis of DGB's are described.

III. CONSTRUCTION OF GAP BREATHERS

The main idea of the numerical method used for construction of breathers is similar to that developed for breathers in monoatomic chains [12,28]. It is based on numerical continuation of an exact solution, which is known for some particular values of system parameters, to other, arbitrary, values of these parameters. In the monoatomic case, usually, an exact breather or multibreather solution with given frequency is taken at zero coupling $C = 0$ (anticontinuous limit), and is
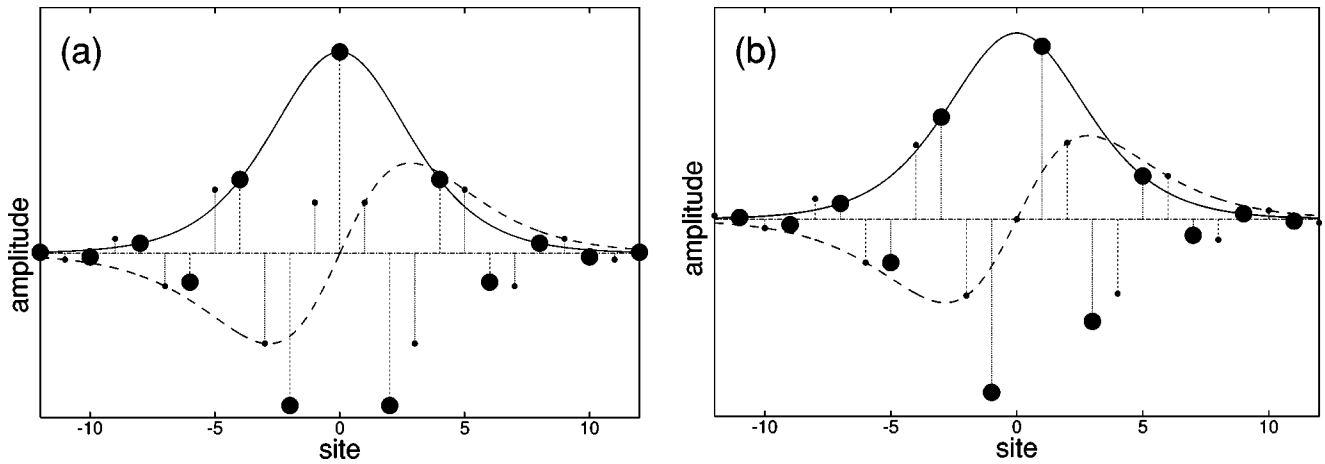
FIG. 2. Displacements of heavy and light atoms in a gap breather: (a) symmetric breather configuration; (b) antisymmetric breather configuration.

then continued to nonzero values of C by a Newton scheme, which uses as initial guess the solution at previous step. As we will show here, in a diatomic chain, such a continuation from anticontinuous limit sometimes cannot be extended to any arbitrary value of the coupling constant because of bifurcations, which can occur to the breather solution when increasing C. To avoid this problem, one can start from some other, nonzero, value of C above the bifurcation point and then continue the breather solution either to higher values of C or back to the bifurcation point. In this case, the trivial exact solution for $C=0$ can not be a good trial one, if the new starting value of C is large enough. Therefore, one should be able to find some other trial solution, which is rather close to the exact breather solution at nonzero value of coupling constant. For this purpose, we use soliton solutions, which were obtained in the continuous limit for gap and out-gap modes in diatomic chains with different types of nonlinearities [5–7]. This limit can be reached at any non-zero value of C by choosing the difference in atom masses to be small enough, so that the width of the gap in the linear wave spectrum will be small. In this case, the frequency and the wave number of the carrier wave in a DGB will be close to the dispersion curves of linear waves, and the breather will be rather nonlocalized (with localization length much larger than the lattice spacing).

The gap boundaries (7) are dependent on the value of coupling constant C. Therefore, if we start with a DGB solution at some given value of the coupling constant $C=C_0$ and try to continue this solution to some $C=C_1$ while keeping the frequency fixed, this frequency can reach one of the gap boundaries at some intermediate point $C=C^*, C_0 < C^* < C_1$. As it was shown in the continuous limit [5–7], the properties of gap solitons are nonsymmetric in the gap: these solitons delocalize and disappear while approaching one of the gap boundaries, but bifurcate into another type of localized excitations—out-gap solitons—at the other gap boundary. In the case of hard nonlinear potential, such a bifurcation will occur at the upper boundary of the gap. Consequently, one can have an additional bifurcation of the breather solution at $C=C^*$. To avoid this effect, we change the breather frequency continuously together with the coupling constant,

so that the following quantity is taken to be fixed:

$$\Delta\omega = \frac{\omega_b - \omega_1(C)}{\omega_2(C) - \omega_1(C)}, \tag{8}$$

which denotes the dimensionless detuning of the breather frequency ω_b from the lower boundary of the gap. This frequency detuning can be considered as the only dynamical parameter of a DGB.

The detailed description of the Newton scheme we use to obtain the breather solution at each step of continuation can be found in Appendix A of Ref. [29].

In this paper, we will consider only those breathers whose frequencies lie inside the gap of linear waves spectrum (gap breathers). For such excitations, we have $0 < \Delta\omega < 1$. We will also consider the simplest case of breathers having tails in the form of standing waves with wave number $k = \pi/2$. In the continuous limit, the corresponding soliton solutions are called "stationary" or "nonmoving" solitons [5–7]. In the case of pure quartic "on-site" nonlinear potential (2), there exists only one type of nonmoving gap soliton [5,7] with the envelope functions of oscillations of heavy and light atoms shown schematically in Fig. 2 (solid and dashed lines, respectively). This gap soliton corresponds to two types of gap breathers in the discrete model: symmetric and antisymmetric breathers with center at heavy or light atom [see Figs. 2(a) and 2(b)] [18]. For linear waves with $k = \pi/2$, neighboring atoms of the same sort oscillate in antiphase having amplitudes with opposite signs. Such a structure will be preserved for nonlinear excitations with the same wave number (see Fig. 2). However, there is always a phase shift of oscillations of light atoms in the center of a DGB, known from the gap soliton solutions in the continuous limit [5–7].

IV. NUMERICAL RESULTS ON CONTINUATION, STABILITY, AND MOBILITY

The numerical investigation was performed for both symmetric and antisymmetric DGB's with different values of fre-

quency detuning $\Delta\omega$, Eq. (8), and most of the results are presented for three distinctive cases: (I) $\Delta\omega = 0.75$, (II) $\Delta\omega = 0.5$, and (III) $\Delta\omega = 0.25$. To obtain numerical solutions, we take a chain with $N = 100$ sites, numbered from $n = -N/2 + 1$ to $n = N/2$, so that the central site (heavy atom in case of symmetric solution and light atom in case of antisymmetric solution) has number $n = 0$. Boundary conditions are periodical. The coefficients of the nonlinear "on-site" potential (2) are taken as $\gamma_2 = \gamma_4 = 1$, and the masses of atoms are $M = 1$, $m = 0.8$. With such a choice of coefficients, the DGB becomes rather nonlocalized at coupling constants as small as $C = 1$ (with localization length of about 50 interatomic distances), so that the soliton solutions obtained in Ref. [5] give good approximations to exact breather solutions when $C \gtrsim 1$.

A. Transition from discretelike to continuouslike solutions

In the anticontinuous limit (at $C = 0$), symmetric breather solutions [see Fig. 2(a)] degenerate into a single oscillating heavy atom with number $n = 0$, while antisymmetric breather solutions [see Fig. 2(b)] degenerate into two neighboring heavy atoms with numbers $n = \pm 1$ oscillating in antiphase. (Note that in the case of hard nonlinear potential, only heavy atoms can oscillate with frequencies inside the gap). We can use these trivial solutions for numerical continuation to nonzero values of coupling constant C. At nonzero coupling, bound vibrations of heavy atoms localize around themselves oscillations of light atoms. The envelope of the light atom oscillations has two symmetric peaks, to the left and to the right of the breather center (see Fig. 2). When the coupling constant C is small enough, these peaks are situated on the light atoms closest to the breather center, i.e., on the atoms with numbers $n = \pm 1$ in the case of symmetric breather solution and on the atoms with numbers $n = \pm 2$ in the case of antisymmetric one. When increasing the coupling constant, the breather solution becomes less localized, approaching the continuous limit soliton solution. Consequently, peaks of light atoms should move further and further away from the central site. Therefore, the continuation of a DGB solution from the anticontinuous to the continuous limit is always accompanied with an infinite number of transformations of the solution, each of them corresponding to a "jump" of the light atoms field peaks from atoms with numbers $n = \pm n_0$ to atoms with numbers $n = \pm (n_0 + 2)$, where $n_0 = 1, 3, 5, \ldots$, for symmetric breathers and $n_0 = 2, 4, 6, \ldots$, for antisymmetric breathers.

The described transitions from one solution to another with different positions of the peaks of light atoms' oscillations can be passed in different ways. In Fig. 3, the dependences of the symmetric breather energy (4) on the value of coupling constant C are shown for different frequencies: (a) $\Delta\omega = 0.25$, (b) $\Delta\omega = 0.5$ (middle of the gap), and (c) $\Delta\omega = 0.75$. When the coupling constant $C = 1$, in all three cases, we have a breather solution with peaks at light atoms with numbers $n = \pm 3$. In contrast, when C is close to zero, the breather solution is extremely localized and has peaks of light atoms' oscillations at $n = \pm 1$. The corresponding structures of the discretelike breather solution at $C = 0.3$ and the
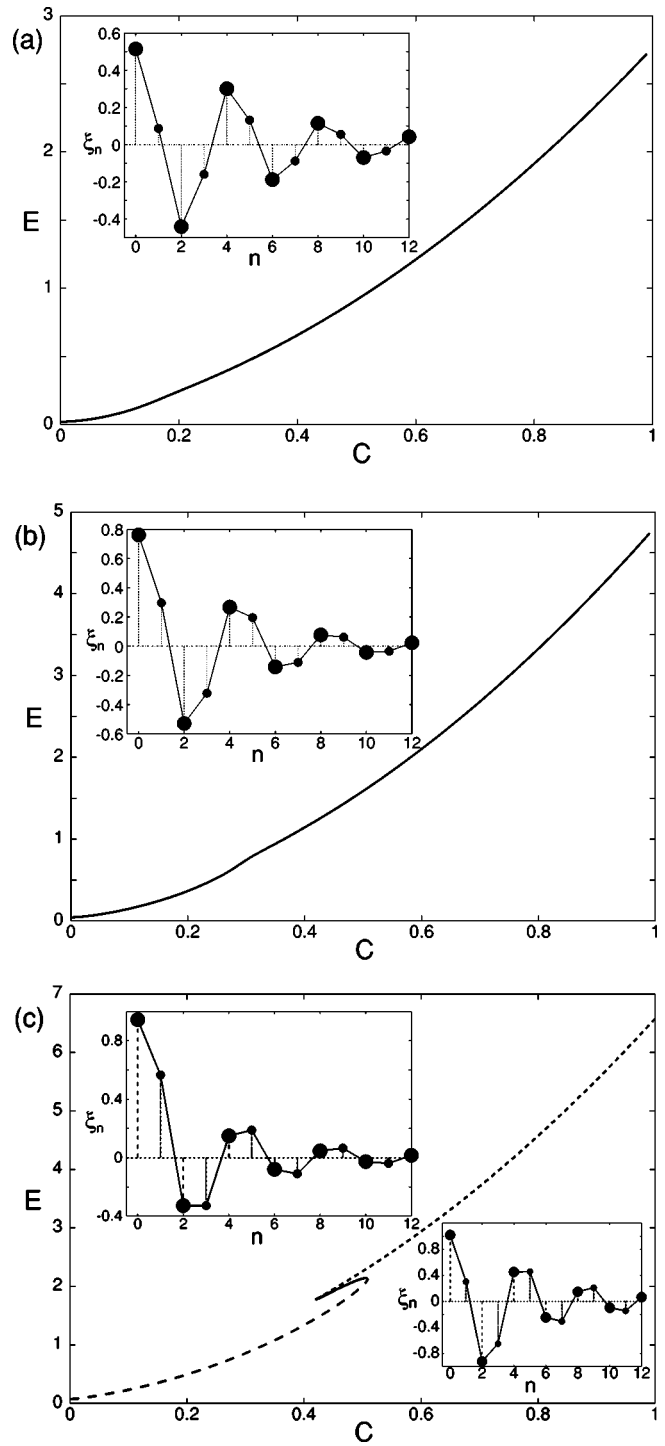

FIG. 3. Dependencies of breather energy E on the value of coupling constant C for symmetric breather solution at different frequencies: (a) $\Delta\omega = 0.25$; (b) $\Delta\omega = 0.50$; (c) $\Delta\omega = 0.75$. Insets in (a) and (b) show the structure of the breather solutions at $C = 0.3$. Insets in (c) show the structure of the breather solutions at $C = 0.3$ (upper inset) and at $C = 0.6$ (lower inset).

continuouslike breather solution at $C = 0.6$ with frequency deviation $\Delta\omega = 0.75$ are shown in the insets in Fig. 3(c). In the case of $\Delta\omega = 0.25$ one has a monotonous continuation in the coupling constant from discretelike to continuouslike solutions. In the middle of the gap (at $\Delta\omega = 0.5$) the continua-

tion is still monotonous, but the second derivative $\partial^2 E/\partial C^2$ is a nonmonotonous function of C, and the transition point $C \approx 0.3$ can be clearly determined from Fig. 3(b). Finally, at $\Delta\omega = 0.75$, there is a region of values of C where three types of solutions coexist simultaneously [see Fig. 3(c)]. The transition from discretelike to continuouslike solutions passes through an intermediate solution, to which the solid line in Fig. 3(c) corresponds. The continuation in the coupling constant from discretelike to continuouslike solution becomes nonmonotonous at some critical value of the frequency detuning $\Delta\omega_c \approx 0.6$, when the curve $E(C)$ becomes vertical at the transition value of C. With further increase of $\Delta\omega$ (i.e., for $\Delta\omega_c < \Delta\omega < 1$), the curve $E(C)$ bends over and the region of multistability appears.

Similar transitions from discretelike to continuouslike solution happen to antisymmetric breathers while increasing the coupling constant C. However, the region of multistability was not observed for antisymmetric breathers at least for $C \leq 5$ and $0.1 \leq \Delta\omega < 1$.

The nonunique character of the transition from discretelike to continuouslike solutions for different frequencies is connected to the effect of competition between two length scales in the breather solution. Indeed, as it can be seen from Fig. 2, the envelopes of oscillations of heavy and light atoms have different localization lengths. Despite the fact that the tails of the breather solution have the same exponential decay in both fields [5–7], characterized by properties of the linearized equations of motion (3), these fields decay in rather different manners closer to the center of the breather. In the continuous small-amplitude approximation the fact of existence of these two length scales becomes rather transparent when approaching the upper boundary of the gap, where the gap soliton transfers into the so-called "algebraic" soliton, with fields decaying as algebraic functions of the coordinate, instead of exponential ones. In the case of hard "on-site" potential, the analytical expression for the envelopes of light and heavy atoms oscillations $f(x)$ and $g(x)$ in the gap soliton can be written as [5,7]:

$$f^2 = \frac{2(1-\Delta\omega)(\Delta\omega)^2 \sinh^2 y}{(\Delta\omega)^2 \sinh^4 y + (1-\Delta\omega)^2 \cosh^4 y}, \qquad (9)$$

$$g^2 = \frac{2(1-\Delta\omega)^2 \Delta\omega \cosh^2 y}{(\Delta\omega)^2 \sinh^4 y + (1-\Delta\omega)^2 \cosh^4 y},$$

where dimensionless variables f, g, and y are defined as:

$$y = \sqrt{\Delta\omega(1-\Delta\omega)} \frac{2C+\gamma_2}{C} \frac{M-m}{M+m} \cdot x,$$

$$\xi_n(t) = \sqrt{\frac{8(2C+\gamma_2)}{3\gamma_4} \frac{M-m}{M+m}} \left\{ f(x \equiv n) \sin\left(\frac{\pi n}{2}\right) \right.$$
$$\left. + g(x \equiv n) \cos\left(\frac{\pi n}{2}\right) \right\} \sin(\omega t).$$

If we denote $z = \sqrt{\Delta\omega/(1-\Delta\omega)}y$, then, in the vicinity of the upper boundary of the gap, that is, in the limit of $\Delta\omega \to 1$, the solution (9) will transfer into an algebraic soliton:

$$f^2 = \frac{2\Delta\omega z^2}{1+z^4}, \qquad (10)$$

$$g^2 = \frac{2\Delta\omega}{1+z^4}.$$

Therefore, light atoms' envelope $f(x)$ decays with coordinate as $1/x$, while heavy atoms' envelope $g(x)$ decays with coordinate as $1/x^2$.

The character of the transition from discretelike to continuouslike breather is dependent on the strength of nonlinear interaction between atoms at the border of two length scales. Similar effects of competition of two length scales were observed earlier in homogeneous models with long-range interactions included [30].

B. Linear stability analysis

Let us consider now in details the linear stability properties of the breather solutions. As usual, to investigate linear stability, we study the time evolution of a small-amplitude perturbation $\{\epsilon_n(0), \dot{\epsilon}_n(0)\}$, which is added at time $t = 0$ to a periodic breather solution $\{\xi_n^{(0)}(t), \dot{\xi}_n^{(0)}(t)\}$ of Eqs. (3), so that we have $\xi_n(t) = \xi_n^{(0)}(t) + \epsilon_n(t)$, $\dot{\xi}_n(t) = \dot{\xi}_n^{(0)}(t) + \dot{\epsilon}_n(t)$. The linearized equations (3) for $\epsilon_n(t)$ can then be written as

$$\mu[1+(-1)^n \delta^2]\ddot{\epsilon}_n + C(2\epsilon_n - \epsilon_{n+1} - \epsilon_{n-1}) + \gamma_2 \epsilon_n$$
$$+ 3\gamma_4(\xi_n^{(0)})^2 \epsilon_n = 0. \qquad (11)$$

The condition of linear stability of the breather solution is fulfilled if and only if the perturbation $\{\epsilon_n(0), \dot{\epsilon}_n(0)\}$ remains bounded in time. To investigate linear stability of time-periodic solutions, one can use Floquet analysis, based on the definition of eigenvalues of a Floquet matrix (Floquet operator) T_0, determined by the following relation:

$$\begin{pmatrix} \{\epsilon_n(t_b)\} \\ \{\dot{\epsilon}_n(t_b)\} \end{pmatrix} = T_0 \begin{pmatrix} \{\epsilon_n(0)\} \\ \{\dot{\epsilon}_n(0)\} \end{pmatrix}, \qquad (12)$$

where $t_b = 2\pi/\omega_b$ is the period of $\{\xi_n^{(0)}(t), \dot{\xi}_n^{(0)}(t)\}$, that is, the period of the breather solution.

Since the Eqs. (11) are time reversible, the breather solution is linearly stable if and only if the eigenvalues of T_0 are on the unit circle (i.e., their modula are equal to unity). In what follows, we will use the term "stable" meaning linear stability of breathers.

1. Symmetric breathers

We will start with symmetric DGB solutions, which have the structure shown in Fig. 2(a). At $C = 0$, when only the central heavy atom is excited, the Floquet matrix T_0 (12) will have one degenerate pair of eigenvalues equal to 1, $N_h - 1$
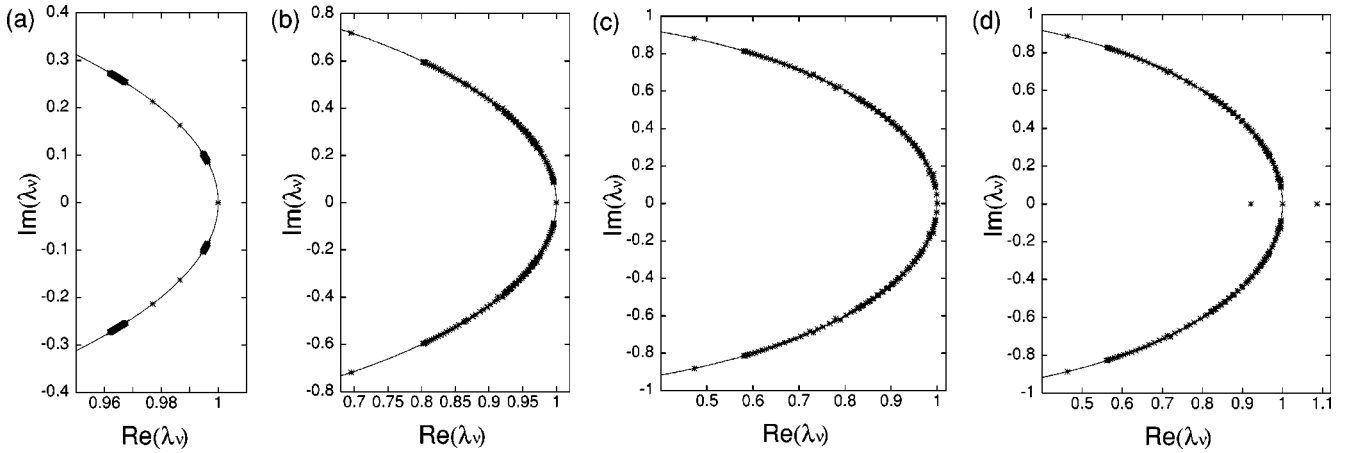
FIG. 4. Imaginary and real parts of Floquet eigenvalues at different values of coupling constant: (a) $C=0.03$; (b) $C=0.23$; (c) $C=0.46$; and (d) $C=0.48$. Frequency detuning is equal to $\Delta\omega=0.75$, corresponding to the discretelike branch of Fig. 3(c).

complex conjugated pairs equal to $e^{\pm i\Theta_h}$, and N_l complex conjugated pairs equal to $e^{\pm i\Theta_l}$ [12]. Here,

$$\Theta_h=2\pi\frac{\omega_h}{\omega_b}, \tag{13}$$

$$\Theta_l=2\pi\frac{\omega_l}{\omega_b},$$

$\omega_h=\sqrt{\gamma_2/M}$, $\omega_l=\sqrt{\gamma_2/m}$ are the frequencies of uncoupled harmonic oscillations of heavy and light atoms correspondingly, ω_b is the frequency of the breather (i.e., the frequency of anharmonic oscillations of the central heavy atom), N_h, N_l are numbers of heavy and light atoms in the chain. Note that if the DGB frequency ω_b is exactly in the middle of the gap [$\omega_b=(\omega_2+\omega_1)/2$], then we will have an additional degeneracy of the Floquet matrix eigenvalues, because $\Theta_h=4\pi-\Theta_l$ in this case.

At nonzero coupling the degeneracy of eigenvalues will be raised, and each of the points on the unit circle $e^{\pm i\Theta_h},e^{\pm i\Theta_l}$ will spread. (The eigenvalue pair at 1 will remain at 1 due to time translation invariance [10].) However, for small values of the coupling constant, all the eigenvalues will remain on the unit circle for generic values of $\Delta\omega$, as the only possibility to leave the unit circle is through a collision of two eigenvalues having opposite Krein signature [12,31], which is determined for each complex conjugated pair of eigenvalues $(\lambda_\nu,\lambda_\nu^*)$ as [29]

$$\kappa(\lambda_\nu)=\text{sign}\left(i\sum_n \epsilon_n^\nu(t)\dot{\epsilon}_n^{\nu*}(t)-\epsilon_n^{\nu*}(t)\dot{\epsilon}_n^\nu(t)\right), \tag{14}$$

where $\epsilon_n^\nu(t)$ is the eigenvector associated with that eigenvalue λ_ν having positive imaginary part. In our case eigenvalues with $\kappa=+1$ correspond to oscillations of light atoms and those with $\kappa=-1$ to oscillations of heavy atoms as $C\to0$.

Such collisions will occur when, while increasing C, the spreading regions of eigenvalues will overlap. The exceptional case is $\Delta\omega=0.5$, when the DGB frequency is in the

middle of the gap. In this case the overlapping of spreading regions will occur at any nonzero value of C, because of the additional degeneracy of eigenvalues at $C=0$ (see above). The imaginary and real parts of the Floquet matrix eigenvalues for different values of coupling C and for the case of $\Delta\omega=0.75$ are plotted in Fig. 4. To reduce the time of numerical calculations, we used the symmetry of the nonlinear potential (2) and performed numerical integrations of the Eqs. (3) and (11) only over a half of the breather period. Therefore, all the angles Θ of eigenvalues in Fig. 4 are twice smaller than their actual values.

All the eigenvalues can be divided into two groups: those having spatially localized and those having spatially extended (over the lattice) eigenvectors. The "extended" eigenvalues are not dependent on the breather spatial configuration and these would be obtained also for the system without breather. Extended eigenvalues are $e^{\pm i\omega(k)t_b}$, where $\omega(k)$ is determined by the linear waves dispersion relation (6) and $t_b=2\pi/\omega_b$. For small values of the coupling constant C, these eigenvalues lie on four arcs of the unit circle [see Fig. 4(a)], defined by the angles

$$\frac{2\pi\omega_o}{\omega_b}\leq\theta\leq\frac{2\pi\omega_1}{\omega_b}, \tag{15}$$

$$\frac{2\pi\omega_2}{\omega_b}\leq\theta\leq\frac{2\pi\omega_m}{\omega_b},$$

and the symmetric arcs with opposite sign of angles. Frequencies ω_o and ω_m are the solutions of Eq. (6) at zero wave number ($k=0$):

$$\omega_{m,o}^2=\frac{\omega_1^2+\omega_2^2}{2}\pm\sqrt{\left(\frac{\omega_2^2-\omega_1^2}{2}\right)^2+\widetilde{\omega}_1^2\widetilde{\omega}_2^2}. \tag{16}$$

The increase of coupling constant will lead to the broadening of each arc and at a certain value of C they will overlap [see Figs. 4(b)–4(d)]. This will cause collisions of extended eigenvalues with generation of instabilities. However, these instabilities should be considered as system size ef-
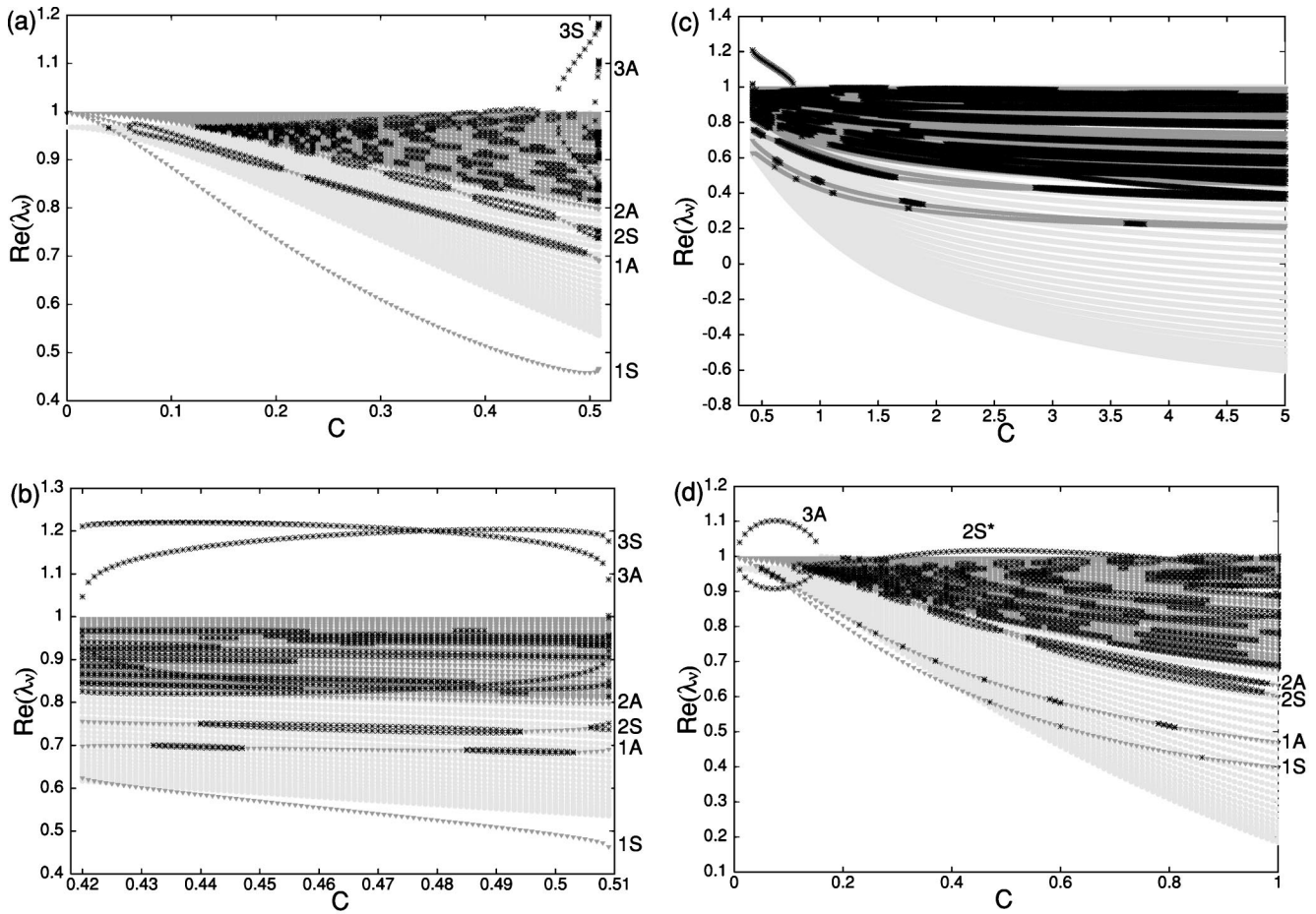
FIG. 5. Real parts of Floquet eigenvalues for the discretelike (a), intermediate (b), continuouslike (c) symmetric breather solutions, and for the antisymmetric breather solution (d) with frequency $\Delta\omega = 0.75$. Light-gray circles correspond to eigenvalues with negative Krein signature, dark-gray triangles correspond to eigenvalues with positive Krein signature, and black stars correspond to unstable eigenvalues.

fects. Indeed, with increase of the system size the arcs of extended eigenvalues will be more dense, and in the limit of an infinite chain these will become continuous. Hence, for larger system sizes, one will have a larger amount of instabilities, produced by collisions of extended eigenvalues. But at the same time, as it was shown in Ref. [32], for any localized solution $\xi_n^{(0)}$, the strength of the extended instabilities will decay with increase of the system size and completely disappear in the limit of an infinite chain.

Eigenvalues associated with localized modes are more essential for the stability analysis. Unlike extended eigenvalues, localized ones have discrete spectrum in the limit of an infinite chain. Their collisions with extended eigenvalues having opposite Krein signature can produce strong instabilities independently of the system size. The corresponding eigenvectors are localized in the region of the breather when the eigenvalues lie outside the extended bands, and their spatial structure is connected to the structure of the breather solution. In the case when a localized eigenvalue resonates with an extended band, yielding a quadruplet of complex eigenvalues off the unit circle, the corresponding eigenvector has tails, but the tail amplitude should decrease when increasing the system size and vanish in the limit of an infinite chain. In Fig. 4(a), one can see two complex conjugated pairs

of localized eigenvalues apart from the bands of extended eigenvalues. With increase of the coupling constant, these pairs penetrate the bands of extended eigenvalues. In Figs. 4(b)–4(d), one of the pairs has passed through the leftmost band, while the other stays inside the bands colliding with extended eigenvalues and producing Krein instabilities. Another mechanism of instability appearance is through a collision of two complex conjugated localized eigenvalues with each other at the point (1,0) in the complex plane [see Figs. 4(c) and 4(d)]. In this case, one pair of unstable eigenvalues appears off the unit circle.

It is convenient to study the linear stability of DGB solutions at different values of the coupling constant by plotting real parts of the Floquet matrix eigenvalues versus C. The most interesting case is the case of $\Delta\omega = 0.75$, where one has a nonmonotonous transition from discretelike to continuouslike breather solution with three coexisting solutions in the vicinity of $C = 0.5$ [see Fig. 3(c)].

In Figs. 5(a)–5(c), the real parts of the eigenvalues are plotted versus coupling for each of the three solutions separately. There we plotted in different gray scales eigenvalues with positive and negative Krein signatures (14) and unstable eigenvalues (with modula outside the unit circle). Most of the instabilities are produced by collisions of eigenvalues
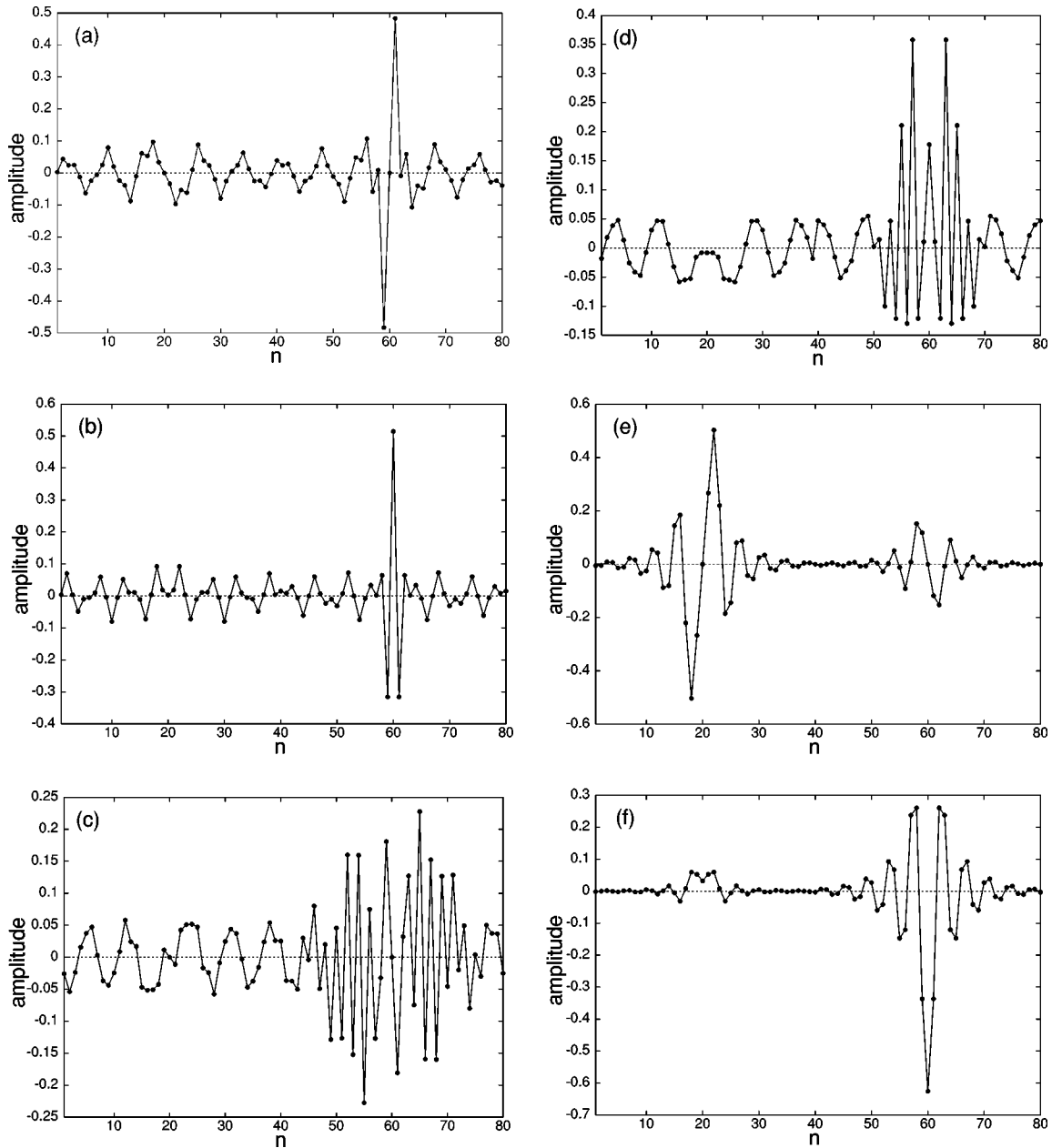
FIG. 6. Real components of the eigenvectors corresponding to localized eigenvalues of Fig. 5(a): (a) $1A$, $C=0.1$; (b) $1S$, $C=0.04$; (c) $2A$, $C=0.41$; (d) $2S$, $C=0.45$; (e) $3A$, $C=0.5075$; and (f) $3S$, $C=0.47$. Components with numbers $n=1,2,\ldots,40$ correspond to the perturbations on the positions of the central 40 particles $(\epsilon_{-19},\epsilon_{-18},\ldots,\epsilon_0,\epsilon_1,\ldots,\epsilon_{20})$, while components with numbers $n=41,42,\ldots,80$ correspond to the perturbations on the velocities of the central 40 particles $(\dot{\epsilon}_{-19},\dot{\epsilon}_{-18},\ldots,\dot{\epsilon}_0,\dot{\epsilon}_1,\ldots,\dot{\epsilon}_{20})$.

belonging to two overlapping continuouslike bands of extended modes with opposite Krein signatures. However, there are also six branches of eigenvalues with localized eigenvectors, representing the purely discrete part of the spectrum of eigenvalues. These branches are marked on Figs. 5(a)–5(d) as $1A,1S,2A,2S,3A,$ and $3S$—numbered in the order these bifurcate from the continuouslike bands and with letters denoting whether the corresponding eigenvector is antisymmetric (A) or symmetric (S) with respect to the breather center site.

Branches $3S$ and $3A$ bifurcate from the continuouslike bands of eigenvalues with positive and negative Krein signa-

tures, correspondingly. When the coupling constant becomes close to the transition region, where the discretelike breather solution transforms into the continuouslike one, each of the eigenvalues $3S$ and $3A$ collides with its complex conjugate at $\theta=0$ and produces two real eigenvalues off the unit circle $(\lambda_1>1$ and $\lambda_2<1)$. With the increase of coupling, these unstable eigenvalues return to the unit circle [see Figs. 5(a) and 5(c)].

Four other branches $1A$, $1S$, $2A$, and $2S$ bifurcate from the continuouslike band of eigenvalues with positive Krein signature. These penetrate the continuouslike band of eigenvalues with opposite Krein signature and seem to stay there
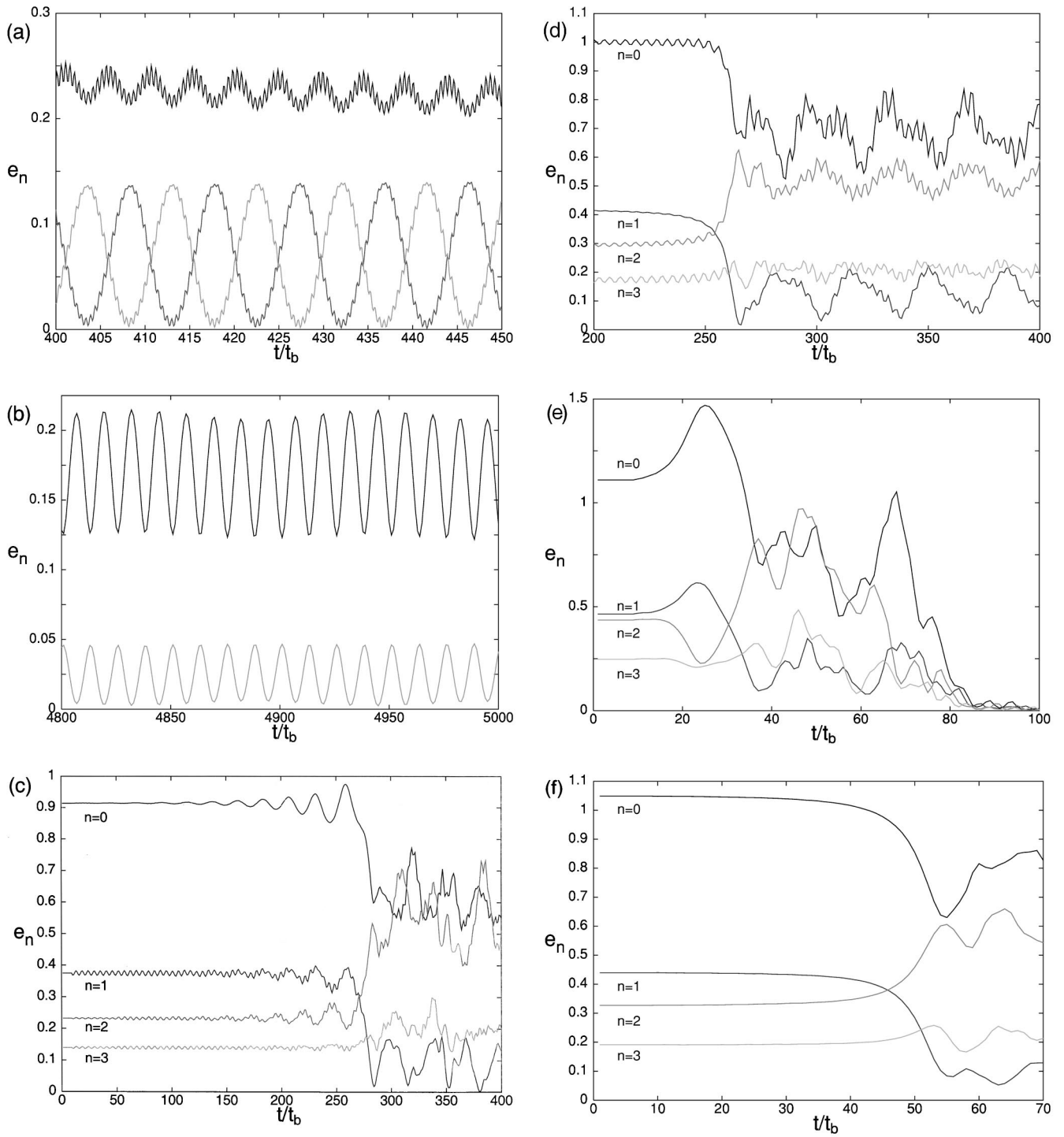
FIG. 7. Breather dynamics with perturbations along the eigenvectors in Fig. 6 for the same solution and parameter values. (a),(b) Energy densities of three central particles ($n=-1,0,1$). The black line corresponds to the energy density of the central particle, the dark gray line corresponds to the energy density of the light atom with number $n=1$, and the light gray line corresponds to the energy density of the light atom with number $n=-1$. In (b), dark gray and light gray lines coincide; (c)–(f) energy densities of four particles to the right of the breather center ($n=0,1,2,3$), plotted in different gray scales. The time unit is equal to the breather period $t_b \equiv 2\pi/\omega_b$.

all the way of continuation of the breather solution to the continuous limit [with the exception of $1S$ which also is outside the continuous band for an interval of intermediate C as shown in Figs. 5(a) and 5(b)]. The subsequent collisions

of an eigenvalue associated with localized modes with the eigenvalues from the continuouslike band will result in the appearence of four complex eigenvalues outside the unit circle ($\lambda, \lambda^*, 1/\lambda, 1/\lambda^*$ with $|\lambda| > 1$). In the limit of an infi-
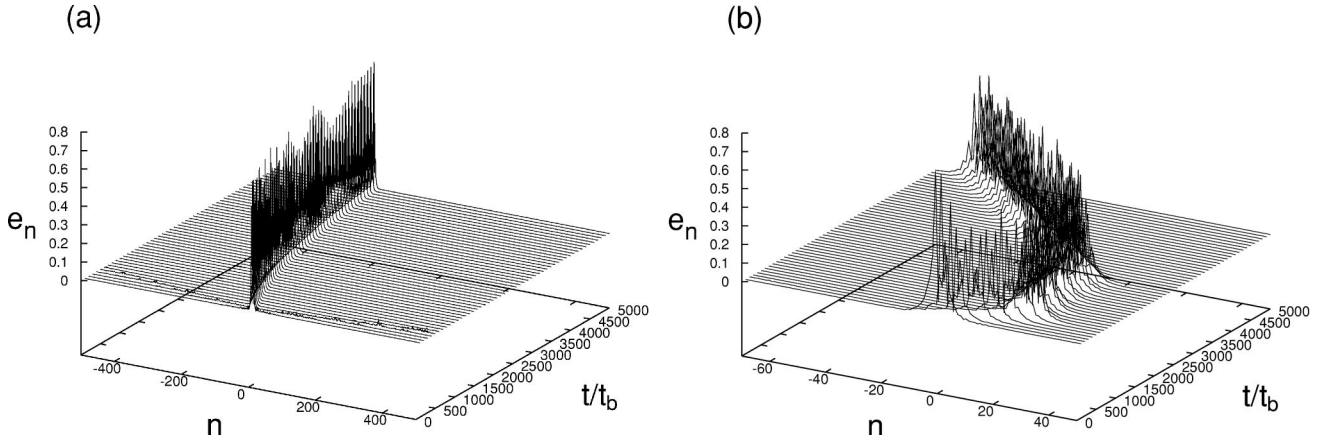
FIG. 8. Breather dynamics with perturbations along the $3A$ (a) and the $3S$ (b) eigenvectors. The values of the coupling constant are (a) $C=0.5075$ and (b) $C=0.47$. Frequency detuning is equal to $\Delta\omega=0.75$. The time unit is equal to the breather period $t_b\equiv2\pi/\omega_b$. The change of the direction of movement of the symmetric breather in (b) is caused by a weak radiation reflected from the boundaries.

nite chain, the phonon bands of eigenvalues will become continuous. Therefore, the number of such collisions will be infinite and the breather will be oscillatorily unstable at any $C>C_0$, where C_0 is the value of the coupling constant at which the $1A$ branch penetrates into the continuous band of eigenvalues with negative Krein signature [see Fig. 5(a)].

To reveal the effect of these six instabilities on the breather solution, we perform numerical simulations of the breather dynamics. We tried to avoid the boundary effects as much as possible. For this purpose, we took a rather big system size—2000 particles—and applied absorbing boundary conditions. The latter allowed us to reduce the reflecting radiation from the boundaries.

Since it is difficult to find some region of values of C where only one of the six instabilities is present, the effect of each particular instability cannot be detected clearly and distinguished from all others by the analysis of the breather dynamics with some arbitrary perturbation added. However, if a perturbation is added along the direction of the eigenvector associated with some particular unstable eigenvalue, one could expect that the effect of this instability will be detected faster than all others. The real components of the eigenvec-

tors associated with the $1A,1S,2A,2S,3A$, and $3S$ instabilities are plotted in Fig. 6. To make these pictures more clear, we plotted only those components corresponding to the perturbations on the 40 central particles (with numbers $n=-19,-18,\ldots,0,\ldots,20$). Components with numbers $n=1,2,\ldots,40$ correspond to the perturbations on displacements of the central particles, while components with numbers $n=41,42,\ldots,80$ correspond to the perturbations on velocities of the central particles. Perturbations on a position and a velocity of the central breather particle have numbers $n=20$ and $n=60$, respectively. Note that the eigenvectors $1A,1S,2A$, and $2S$ are associated with the unstable eigenvalues resonating with extended eigenvalues of the continuouslike bands. Therefore, these eigenvectors are extended over the lattice (but the amplitude of the tails will decrease when increasing the system size). In contrast, the eigenvectors $3A$ and $3S$ are localized on the central breather particles, being associated with unstable real eigenvalues lying outside the continuouslike bands.

The most general effect of all the instabilities is, at the final stage, a transition of the initial periodic DGB solution into more stable "quasiperiodic" localized solutions with os-
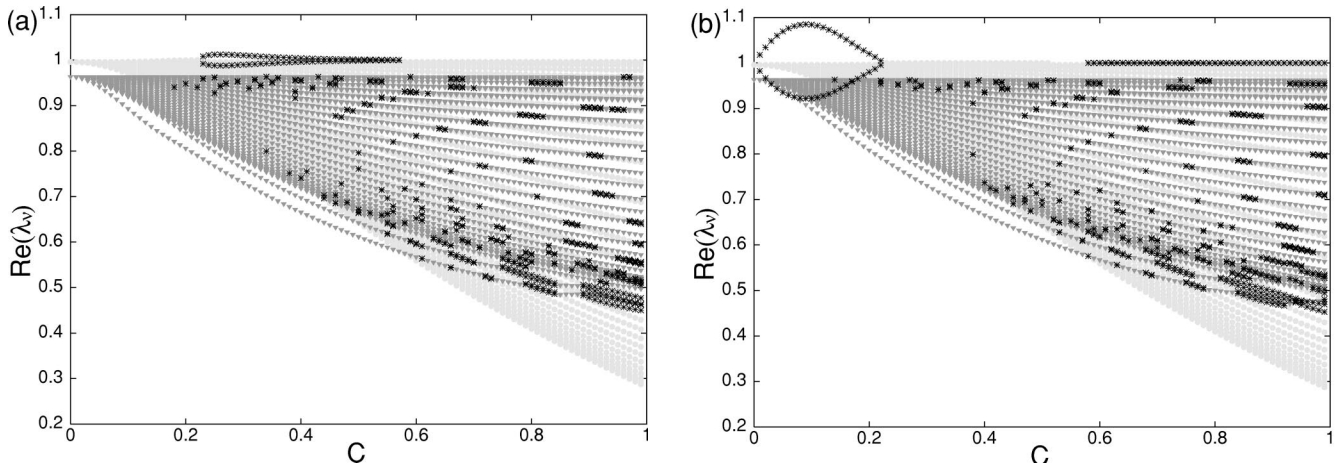

FIG. 9. Real parts of Floquet eigenvalues for symmetric (a) and antisymmetric (b) breather solutions, $\Delta\omega=0.25$.
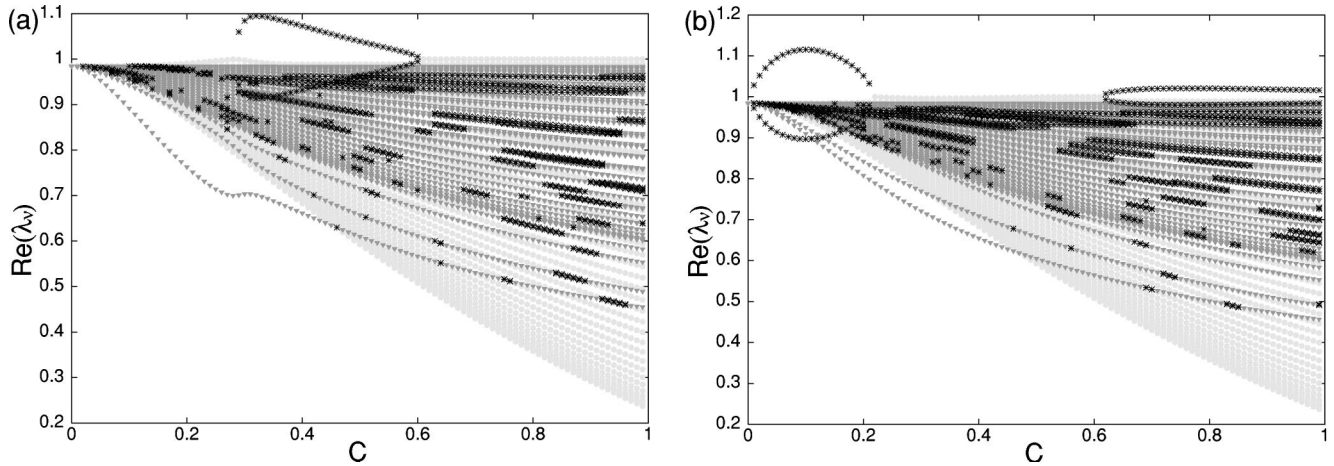
FIG. 10. Real parts of Floquet eigenvalues for symmetric (a) and antisymmetric (b) breather solutions, $\Delta\omega = 0.50$.

cillations of the energy density (5) between central and neighboring particles (see Fig. 7). The basical structure of these oscillations for the cases of symmetric and antisymmetric perturbations becomes rather transparent while approaching the anticontinuous limit where the DGB solution is extremely localized. In Figs. 7(a) and 7(b), the structure of the intrinsic oscillations is shown for $C = 0.1$ and $C = 0.04$ as a result of the breather dynamics with perturbations along the $1A$ and $1S$ eigenvectors, respectively. In both cases, we have energy density oscillations between the central heavy particle (with number $n = 0$) and the two neighboring light ones ($n = \pm 1$). The energy densities of the light particles oscillate in phase when the instability is symmetric, and in antiphase when the instability is antisymmetric. When the coupling constant is large enough, these oscillations in the case of antisymmetric instability lead to a transition to the antisymmetric breather configuration centered on a light atom with zero amplitude and with two neighboring heavy atoms oscillating in antiphase with equal amplitudes [see Fig. 2(b)]. Such transitions occur at $C = 0.41$ and $C = 0.5075$ in the breather dynamics with perturbations along the $2A$ and $3A$ eigenvectors correspondingly [see Figs. 7(c) and 7(e)]. In the case of the $2A$ instability, the center of the breather jumps to the light atom with $n = 1$ (or to the light atom with $n = -1$ depending on the initial perturbation), while two neighboring heavy atoms $n = 0,2$ possess almost the same energy densities [Fig. 7(c)]. A similar scenario happens in the case of the $3A$ instability, but now the breather possesses rather good mobility (since this type of instability is connected with the transition into the continuouslike DGB solution). The resulting movement of the breather is shown in Fig. 8(a). Note that in the case of the $3A$ instability, the perturbation develops without any oscillations of energy densities of particles, since the corresponding unstable eigenvalue is real.

The effect of the symmetric $2S$ and $3S$ instabilities is a transition of the breather solution into a continuouslike one. In both cases the peak of oscillations of light atoms jumps from $n = \pm 1$ to $n = \pm 3$ [see Figs. 7(d) and 7(f)]. An interesting scenario occurs for $C = 0.47$ with perturbation along the $3S$ eigenvector. At this value of coupling constant, the discretelike DGB solution also has the $1A$ antisymmetric in-

stability [see Fig. 5(a)], but this instability is rather weak as compared to the symmetric $3S$ instability. As a result of addition of a small perturbation along the $3S$ eigenvector, the breather solution transfers into a continuouslike one with peaks of the light atoms at $n = \pm 3$. But this solution has a rather strong antisymmetric $3A$ instability at coupling $C = 0.47$ [see Fig. 5(c)] together with a good mobility. Therefore, the following transformation into antisymmetric solution occurs solely from numerical truncation error and the breather starts to move along the chain [see Fig. 8(b)].

Changing the breather frequency, the two bands of extended eigenvalues will change their relative positions (see Fig. 9 for $\Delta\omega = 0.25$ and Fig. 10 for $\Delta\omega = 0.5$). But all the above described instabilities will remain (at least for not too small frequencies: $\Delta\omega \gtrsim 0.1$) except the symmetric instability $3S$, which can disappear in some cases (we do not discuss here the limiting case of $\Delta\omega \to 0$, which is numerically difficult due to size divergence). This instability exists at those values of the frequency detuning $\Delta\omega$ and the coupling constant C, where for the breather energy one has $dE/d\omega_b < 0$, which is similar to the Vakhitov-Kolokolov linear stability criterion derived for soliton solutions of the generalized nonlinear Schrödinger equations [33]. In Fig. 11, the dependencies of the breather energy on the frequency detuning $\Delta\omega$ are plotted as the results of numerical continuation of the symmetric DGB solutions at different fixed values of the coupling constant while changing $\Delta\omega$. A section of the curve $E(\Delta\omega)$ with negative slope appears in Fig. 11(c) at frequencies $\Delta\omega > 0.5$. Consequently, one should expect the appearance of the $3S$ instability in the upper half of the gap.

We would like to add here, that in each case, the continuation in coupling is performed up to some finite value of coupling C (because of the size-divergence problems—DGB solutions become less localized when increasing C). With further increase of coupling, more localized modes can bifurcate from the bottom of the band of extended eigenvalues with positive Krein signature, as the central part of DGB solution will occupy a larger number of particles. However, possible new oscillatory instabilities, connected to these localized modes, should be analogous to the above described $1A, 1S, 2A$, and $2S$ instabilities.
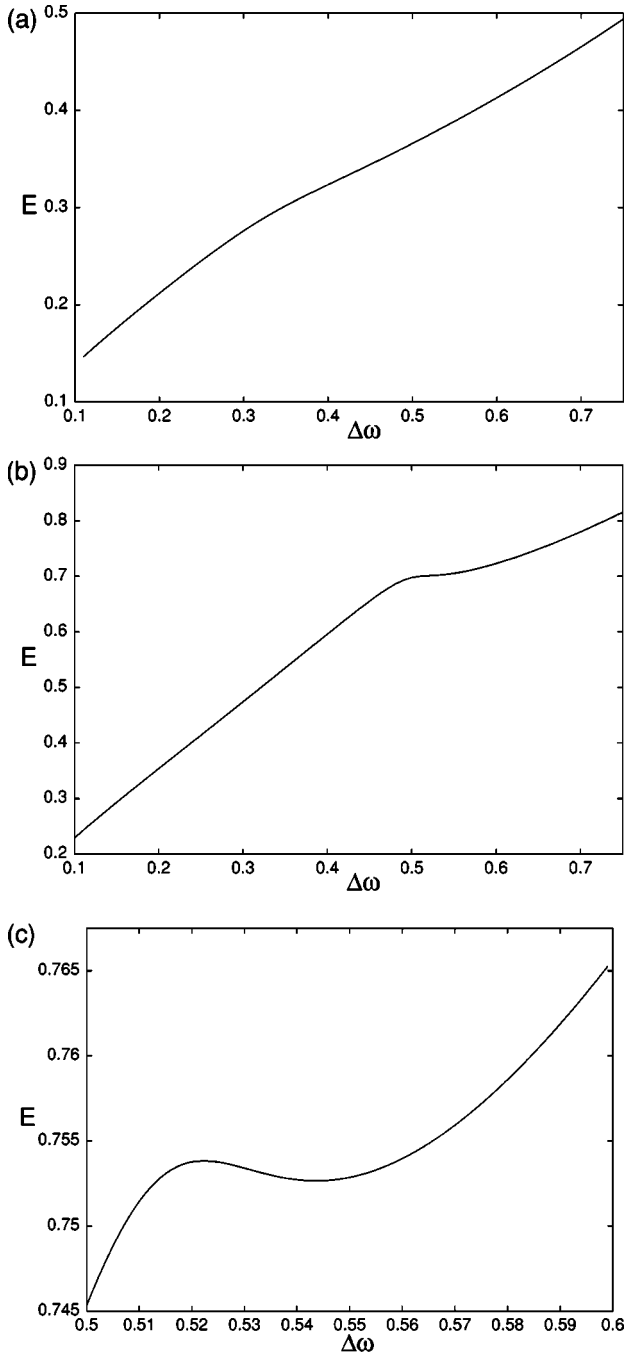
(a)

(b)

(c)

FIG. 11. Dependencies of the energy of the symmetric breather solutions on the frequency detuning $\Delta\omega$ at different fixed values of the coupling constant: (a) $C=0.2$; (b) $C=0.29$; and (c) $C=0.3$.
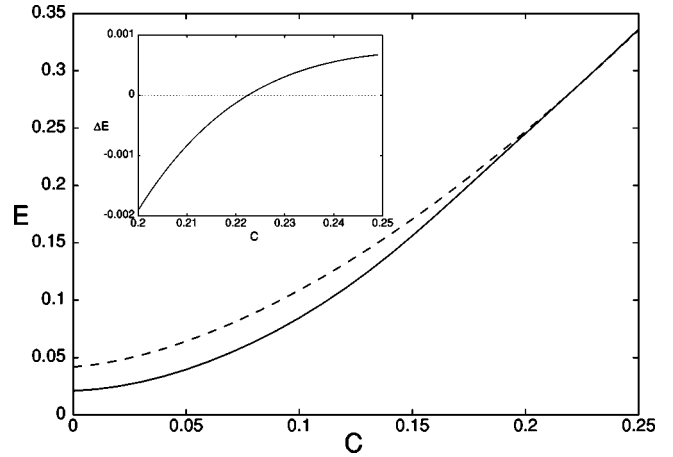

FIG. 12. Dependencies of energies of the symmetric (solid lines) and the antisymmetric (dashed lines) breathers on the value of the coupling constant for the frequency detuning equal to $\Delta\omega=0.25$. In the inset, the difference between the energies of the symmetric and the antisymmetric breathers $\Delta E=E_{sym}-E_{asym}$ is plotted vs coupling.

2. Antisymmetric breathers

An antisymmetric DGB solution has the structure shown in Fig. 2(b). In the anticontinuous limit (at $C=0$), such a breather degenerates into two neighboring heavy atoms oscillating in antiphase. The light atom in the center of the breather always has zero amplitude. The structure of the Floquet eigenvalues spectrum in the anticontinuous limit for the antisymmetric DGB solution is basically the same as for the symmetric one. However, now there are two pairs of eigenvalues equal to 1, as in the antisymmetric DGB solution two

atoms are excited at $C=0$. One of these pairs leaves the unit circle immediately when C becomes nonzero, producing a nonoscillatory instability at small values of coupling [see Fig. 5(d), 9(b), and 10(b)]. The same instability was observed for antisymmetric breathers in diatomic FPU chains [19,21]. The instability is similar to the $3A$ instability for symmetric breathers. It has a localized antisymmetric eigenvector which tends to transform the solution into a symmetric one, which always possesses a lower energy at small values of the coupling being more localized (see, for example, Fig. 12).

At frequency detuning $\Delta\omega=0.75$, another specific instability is observed, which is denoted as $2S^*$ in Fig. 5(d). This symmetric oscillatory instability is similar to the above described $1S$ and $2S$ instabilities. The localized eigenvalue associated with $2S^*$ also bifurcates from the bottom of the band of extended eigenvalues with positive Krein signature. However, after collision with an extended eigenvalue from the other band, it produces a rather strong instability and the unstable eigenvalues remain outside the unit circle all the way of continuation in coupling up to the value of coupling constant $C\approx4$.

The rest of the structure of the extended and localized eigenvalue spectra is qualitatively the same as in the case of symmetric breathers. Antisymmetric breathers have all the above described localized instabilities, except the $3S$ instability which was not observed at least for $C\lesssim5$ and $0.1\lesssim\Delta\omega<1$. Higher values of C, as well as the limiting case of $\Delta\omega\to0$, were not investigated because of the size-divergence problems (the DGB solution becomes rather non-localized).

Of principal interest are those values of the coupling constant and the frequency detuning, at which symmetric and antisymmetric breathers have real instabilities simultaneously. In such a case of "inversion of stability" [27], breathers can possess extremely good mobility despite the fact that these can still be rather localized. As an example of
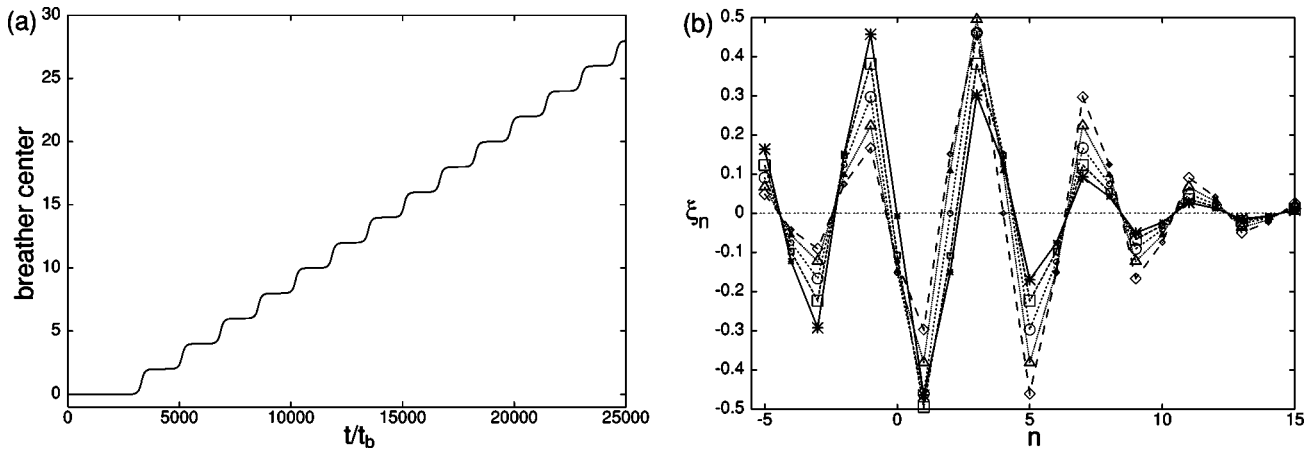
FIG. 13. Dynamics of the antisymmetric breather without perturbation (with only numerical truncation error), $C = 0.22$, $\Delta\omega = 0.25$: (a) position of the breather center, with time unit equal to the breather period $t_b = 2\pi/\omega_b$; (b) displacements of the 20 particles with numbers $n = -5, -4, \ldots, 0, \ldots, 14, 15$ at different time instants: * indicates displacements at $t = 2400 t_b$ (center of the DGB is at $n = 0$); □ displacements at $t = 3307 t_b$ (center of the DGB is at $n = 1$); ○ displacements at $t = 4215 t_b$ (center of the DGB is at $n = 2$); △ displacements at $t = 5122 t_b$ (center of the DGB is at $n = 3$); and ◇ displacements at $t = 6000 t_b$ (center of the DGB is at $n = 4$). Large and small symbols denote the displacements of heavy and light atoms, respectively.

such a mobility of gap breathers, we present here the results of dynamics of the antisymmetric breather with frequency detuning $\Delta\omega = 0.25$ at coupling $C = 0.22$. At these values of coupling and frequency, both the antisymmetric and the symmetric breather solutions have the $3A$ instability (see Fig. 9), which transforms them into each other. And these symmetric and antisymmetric breathers have almost the same energies (see Fig. 12), so that these can transform into each other rather easily and without any significant radiation. The resulting movement is shown in Fig. 13. Similar results were obtained for the dynamics of the symmetric breather.

V. CONCLUSIONS

We have investigated the linear stability properties of gap breathers in a one-dimensional diatomic chain with nonlinear quartic on-site potential. The coupling constant was changed continuously from $C = 0$ (anticontinuous limit) to the values, at which the localization lengths of the breather solutions are much larger than the lattice spacing (continuous limit). We have shown that in the limit of an infinite chain, gap breathers are generally unstable in the full regime of continuation from the anticontinuous to the continuous limit except the regions of values of the coupling constant near $C = 0$. However, the limiting case of $\Delta\omega \rightarrow 0$ is not discussed in this paper. This case is numerically difficult due to size-divergence problem, it is a matter of future investigation.

At small values of the coupling constant, symmetric gap breathers were found to be linearly stable, while antisymmetric gap breathers were unstable. These results are in a good agreement with the results of linear stability analysis of DGB's in diatomic FPU chains in the anticontinuous limit within the RWA approximation [19,21].

Six different types of instabilities of symmetric and antisymmetric breathers were revealed and the effects of each of them on the DGB solutions were investigated. Two of these

instabilities have real eigenvalues. One of them ($3S$) is connected to the transition of a breather solution from less to more localized with a jump of the peaks of light atom oscillations. Another real instability is similar to the Peierls-Nabarro translation mode in monoatomic chains. In the continuous limit, these instabilities will disappear. Four other instabilities are of the oscillatory type with complex eigenvalues. These are produced by collisions of localized eigenvalues with extended eigenvalues. The former penetrate the band of extended eigenvalues with opposite Krein signatures and seem to stay there all the way of continuation to the continuous limit. Therefore, in the continuous limit, gap solitons should be oscillatorily unstable. However, at frequencies close to the lower boundary of the gap in the linear wave spectrum, the branches of localized eigenvalues can asymptotically return to the band of extended eigenvalues with the same Krein signatures, from which these bifurcated. In this case, gap solitons will be linearly stable in the continuous limit. Similar results of linear stability analysis were obtained for gap solitons in the continuous massive Thirring models [24–26].

The regime of inversion of stability of gap breathers was studied. In this regime, both symmetric and antisymmetric DGB's possess real instabilities, having approximately the same energies. This results in good mobility of a breather without any significant radiation of energy. Such a mobility was shown in the dynamics of an antisymmetric gap breather.

[1] W. Chen and D.L. Mills, Phys. Rev. Lett. **58**, 160 (1987).

[2] J. Coste and J. Peyraud, Phys. Rev. B **39**, 13 086 (1989); **39**, 13 096 (1989).

[3] C.M. Sterke and J.E. Sipe, in *Progress in Optics*, edited by E. Wolf (Elsevier, Amsterdam, 1994), Vol. XXXIII, p. 203.

[4] A.B. Aceves, Chaos **10**, 584 (2000).

[5] Yu.S. Kivshar and N. Flytzanis, Phys. Rev. A **46**, 7972 (1992).

[6] O. A. Chubykalo, A. S. Kovalev, and O. V. Usatenko, Phys. Rev. B **47**, 3153 (1993).

[7] A.S. Kovalev, O.V. Usatenko, and A.V. Gorbatch, Phys. Rev. E **60**, 2309 (1999).

[8] A.S. Kovalev, O.V. Usatenko, and A.V. Gorbach, Phys. Solid State **43**, 1665 (2001).

[9] A.V. Gorbach, A.S. Kovalev, and O.V. Usatenko, Low Temp. Phys. **27**, 579 (2001).

[10] R.S. MacKay and S. Aubry, Nonlinearity **7**, 1623 (1994).

[11] S. Flach and C.R. Willis, Phys. Rep. **295**, 181 (1998).

[12] S. Aubry, Physica D **103**, 201 (1997).

[13] R. Livi, M. Spicci, and R.S. MacKay, Nonlinearity **10**, 1421 (1997).

[14] T. Cretegny, R. Livi, and M. Spicci, Physica D **119**, 88 (1998).

[15] A.V. Zolotaryuk, P. Maniadis, and G.P. Tsironis, Physica B **296**, 251 (2001).

[16] P. Maniadis, A.V. Zolotaryuk, and G.P. Tsironis, Phys. Rev. E **67**, 046612 (2003).

[17] A.A. Sukhorukov and Yu.S. Kivshar, Opt. Lett. **27**, 2112 (2002).

[18] O.A. Chubykalo and Yu.S. Kivshar, Phys. Rev. E **48**, 4128 (1993); **49**, 5906 (1994).

[19] S.A. Kiselev, S.R. Bickham, and A.J. Sievers, Phys. Rev. B **48**, 13 508 (1993).

[20] M. Aoki, S. Takeno, and A.J. Sievers, J. Phys. Soc. Jpn. **62**, 4295 (1993).

[21] S.A. Kiselev, S.R. Bickham, and A.J. Sievers, Phys. Rev. B **50**, 9135 (1994).

[22] A. Franchini, V. Bortolani, and R.F. Wallis, Phys. Rev. B **53**, 5420 (1996).

[23] A. Franchini, V. Bortolani, and R.F. Wallis, J. Phys.: Condens. Matter **14**, 145 (2002).

[24] I.V. Barashenkov, D.E. Pelinovsky, and E.V. Zemlyanaya, Phys. Rev. Lett. **80**, 5117 (1998).

[25] A. De Rossi, C. Conti, and S. Trillo, Phys. Rev. Lett. **81**, 85 (1998).

[26] I.V. Barashenkov and E.V. Zemlyanaya, Comput. Phys. Commun. **126**, 22 (2000).

[27] T. Cretegny, Ph.D. thesis, École Normale Supérieure de Lyon, France, 1998.

[28] J.L. Marín and S. Aubry, Nonlinearity **9**, 1501 (1996).

[29] G. Kopidakis and S. Aubry, Physica D **130**, 155 (1999).

[30] P.L. Christiansen, Y.B. Gaididei, F.G. Mertens, and S.F. Mingaleev, Eur. Phys. J. B **19**, 545 (2001).

[31] V.I. Arnold and A. Avez, *Ergodic Problems of Classical Mechanics* (W.A. Benjamin Inc., New York, 1968), Appendix 29.

[32] J.L. Marín and S. Aubry, Physica D **119**, 163 (1998).

[33] M.G. Vakhitov and A.A. Kolokolov, Radiophys. Quantum Electron. **16**, 783 (1973).